

Structural characterization of agmatine at physiological conditions

Antonio Toninello · Valentina Battaglia · Mauro Salvi ·
Rita Calheiros · M. Paula M. Marques

Received: 13 April 2005 / Accepted: 23 September 2005 / Published online: 19 May 2006
© Springer Science+Business Media, Inc. 2006

Abstract The present work aims at determining the *structure–activity relationships* (SAR's) which rule the biological function of agmatine (4-(aminobutyl)guanidinium, AGM), a biogenic amine produced by decarboxylation of arginine. Its structural preferences, both as an isolated molecule and in aqueous solution (namely at physiological conditions) were ascertained, by vibrational (Raman) spectroscopy coupled to theoretical (density functional) calculations. An evaluation of mitochondrial functions (membrane potential ($\Delta\Psi$), mitochondrial swelling, and cytochrome c release) in rat liver mitochondria (RLM) was also carried out. The results thus obtained, coupled to the conformational analysis performed for the distinct polyamine protonation states, allowed to individualize the agmatine structures which interact with the mitochondrial site responsible for its transport and for the protection against mitochondrial permeability transition (MPT) induction, as

well as to gain information on the specific mechanisms involved.

Keywords Agmatine · Physiological structure · Mitochondrial permeability transition · DFT calculations · Raman spectroscopy

Introduction

Agmatine (4-(aminobutyl)guanidinium, AGM, Fig. 1), is a biogenic amine produced by decarboxylation of L-arginine by arginine decarboxylase (ADC). The metabolic pathway of agmatine synthesis, long known to be present in bacteria and plants, has lately also been demonstrated in mammalian tissues [1]. A large number of evidence has been reported regarding the wide range of physiological functions carried out by agmatine [2]. In fact, this polyamine was found to act as a neurotransmitter or neuromodulator [3] and bind to imidazoline and α_2 -receptors [4, 5], and it can stimulate insulin release [6] and induce catecholamine [3]. In addition, agmatine may behave as an antiproliferative agent and tumor suppressor [7–10], by inhibiting polyamine biosynthesis and thus regulating cell proliferation (e.g., in rat hepatoma cells [11]), as well as by modulating apoptosis (e.g., in hepatocytes [12]).

Besides being synthesized *in situ*, agmatine can also be taken up from exogenous sources through the diet, and accumulated in the cells and the subcellular organelles by means of specific protein transporters [13–15], which have not yet been identified at a molecular level. As accounted for other biogenic polyamines, the activity of agmatine as a transportable cation and biological effector can be significantly influenced by its structural preferences. Thus, the study of

A. Toninello · V. Battaglia · M. Salvi
Dipartimento di Chimica Biologica,
Università degli Studi di Padova,
35121 Padova, Italia

R. Calheiros · M. P. M. Marques
Unidade de Química-Física Molecular,
Universidade de Coimbra,
Coimbra, Portugal

M. P. M. Marques (✉)
Departamento de Bioquímica,
Faculdade de Ciências e Tecnologia,
Universidade de Coimbra,
Apartado 3126, 3001-401,
Coimbra, Portugal
e-mail: pmc@ci.uc.pt

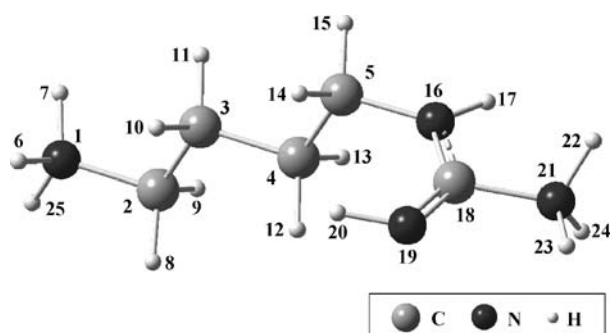


Fig. 1 Schematic representation of the agmatine molecule, in the totally protonated form. (The atom numbering is included)

its conformational characteristics is of the utmost importance for the understanding of the *structure–activity relationships* (SAR's), which rule AGM's diverse biological functions.

The goal of the present work is to better understand the role of agmatine in biological systems (e.g., mitochondria) in the light of a thorough conformational analysis of the polyamine, both in the solid and in aqueous solution, for AGM distinct protonation states. Vibrational (Raman) spectroscopy combined to theoretical methods (density functional calculations) were used for the structural study, while biological assays were carried out in rat liver mitochondria (RLM) preparations. In this regard, the phenomenon of mitochondrial permeability transition (MPT) has been taken into account.

MPT is due to the opening of a high conductance channel, the transition pore, in the mitochondrial membrane. This phenomenon takes place when a large amount of Ca^{2+} accumulates in mitochondria, together with an inducing agent, e.g., phosphate or a pro-oxidant compound. The production of reactive oxygen species, though the oxidation of critical thiol groups, and the interaction of Ca^{2+} with specific sites of the adenine nucleotide translocase, are then responsible for triggering MPT. This is characterized by a collapse of $\Delta\Psi$, matrix swelling, release of endogenous cations, and oxidation of sulphhydryl groups, glutathione, and pyridin nucleotides. All these events add to a redox catastrophe and a bioenergetic collapse [16]. Indeed, the swelling undergone by mitochondria is responsible for outer membrane rupture and the consequent release of soluble factors such as cytochrome *c* (responsible for caspase activation), the final result being apoptosis induction (for a review see [17]).

Experimental section

Chemicals

Agmatine, anticytochrome *c* antibody (Pharmigen), biuret, bovine serum albumine (BSA), ethylenediaminetetraacetic

acid (EDTA), ethyleneglycol-bis(2-aminoethylether)-*N,N,N',N'*-tetraacetic acid (EGTA), carbonyl cyanide *p*-trifluoromethoxyphenyl-hydrazone (FCCP), rutenone, ruthenium red, SDS-PAGE, succinate, tetraphenylphosphonium cation (TPP^+), as well as the Centrikon membranes (Amicon), were purchased from Sigma–Aldrich.

Biological assays

Mitochondrial preparations

RLM were isolated by conventional differential centrifugation, in a buffer medium containing 250 mmol dm^{-3} sucrose, 5 mmol dm^{-3} Hepes (pH 7.4), and 1 mmol dm^{-3} EGTA. EGTA was omitted from the final washing solution [18]. Protein content was measured by the biuret method with bovine serum albumin as a standard [19].

Standard incubation procedures

RLM (1 mg protein/mL) were incubated in a water-jacketed cell at 20°C . The standard medium contained 200 mmol dm^{-3} sucrose, 10 mmol dm^{-3} Hepes (pH 7.4), 5 mmol dm^{-3} succinate, and $1.25 \mu\text{mol dm}^{-3}$ rotenone. Variations and/or other additions are described for each particular experiment presented.

Determination of mitochondrial functions

The membrane potential ($\Delta\Psi$) was calculated on the basis of distribution of the lipid-soluble tetraphenylphosphonium cation (TPP^+) through the inner mitochondrial membrane. This was measured with a homemade TPP^+ -specific electrode (according to published procedures [20]).

The mitochondrial swelling was determined by measuring the apparent absorbance change of the mitochondrial suspension at 540 nm , using a Kontron Uvikon mo. 922 spectrophotometer, equipped with a thermostatic control.

The protein sulphhydryl group oxidation assay was performed as described in the literature [21].

*Detection of cytochrome *c* release*

RLM (1 mg protein/mL) were incubated at 20°C for 15 min in the standard medium, with appropriate additions. The reaction mixtures were then centrifuged at $13,000 \times g$ for 10 min, at 4°C , in order to obtain mitochondrial pellets. The supernatant fractions were further spun at $100,000 \text{ g}$ for 15 min, at 4°C (in view of eliminating mitochondrial membrane fragments) and five times concentrated by ultrafiltration through Centrikon membranes (Amicon), at 4°C . Aliquots of these concentrated supernatants were then subject to 15%-SDS-PAGE (sodium dodecylsulphate-polyacrylamide gel electrophoresis) for cytochrome *c*, and analyzed by

Western Blotting using a mouse anticytochrome c antibody (Pharmingen).

Theoretical calculations

The density functional calculations—full geometry optimization and calculation of the harmonic vibrational frequencies—were performed using the GAUSSIAN 98W program [22] within the Density Functional Theory (DFT) approach, in order to properly account for the electron correlation effects (particularly important in this kind of systems). The widely employed hybrid method denoted by B3LYP [22–28], which includes a mixture of HF and DFT exchange terms and the gradient-corrected correlation functional of Lee *et al.* [29, 30], as proposed and parametrized by Becke [31, 32], was used, along with the double-zeta split valence basis set 6-31G** [33, 34].

Molecular geometries were fully optimized by the Bery algorithm, using redundant internal coordinates [35]: the bond lengths to within *ca.* 0.1 pm and the bond angles to within *ca.* 0.1°. The final root-mean-square (rms) gradients were always less than 3×10^{-4} hartree bohr⁻¹ or hartree radian⁻¹. No geometrical constraints were imposed on the molecules under study.

Mulliken atomic charges were calculated for the different protonation forms of the agmatine molecule. The relative populations were determined according to the Boltzmann distribution (at 25°C), based on the relative conformational energies yielded by the geometry optimization. The calculated wavenumbers above 400 cm⁻¹ were scaled using a factor of 0.9614 according to Scott and Radom [36], before comparing them with the experimental data.

The solvent effect (water) was simulated by performing Self-Consistent Reaction Field (SCRF) calculations. A continuum model—the Integral Equation Formalism (IEF) [37–39] version of Tomasi's Polarized Continuum Model (PCM) [40–42]—was used. This approach defines the molecular cavity as the union of a series of interlocking spheres centered on the distinct atoms of the system.

Raman spectroscopy

The Raman spectra were obtained at room temperature, for both the pure solid and the aqueous solutions of agmatine, on a triple monochromator Jobin-Yvon T64000 Raman system (0.640 m, *f*/7.5) with holographic gratings of 1800 grooves mm⁻¹. The detection system was a nonintensified CCD (Charge Coupled Device). The entrance slit was set to 200 μm and the slit between the premonochromator and the spectrograph was opened to 14.0 mm. The 514.5 nm line of an Ar⁺ laser (Coherent, model Innova 300) was used as excitation radiation, providing 60 to 200 mW

at the sample position. Each spectrum is the sum of about three scans for the solid samples and 10–15 scans for the solutions. Under the above-mentioned conditions, the error in wavenumbers was estimated to be within 1 cm⁻¹. Samples were sealed in Kimax glass capillary tubes of 0.8 mm inner diameter.

For all agmatine aqueous solutions, the pH was adjusted with NaOH and/or HCl, the presence of the Na⁺ and Cl⁻ ions leading to a better mimetization of the physiological conditions.

The spectra of the analogous polyamines dien (H₂N(CH₂)₂NH(CH₂)₂NH₂) and propen (H₂N(CH₂)₃NH(CH₂)₃NH₂), in the solid N-protonated form, were also obtained, in order to better assign the agmatine features.

Statistical analysis

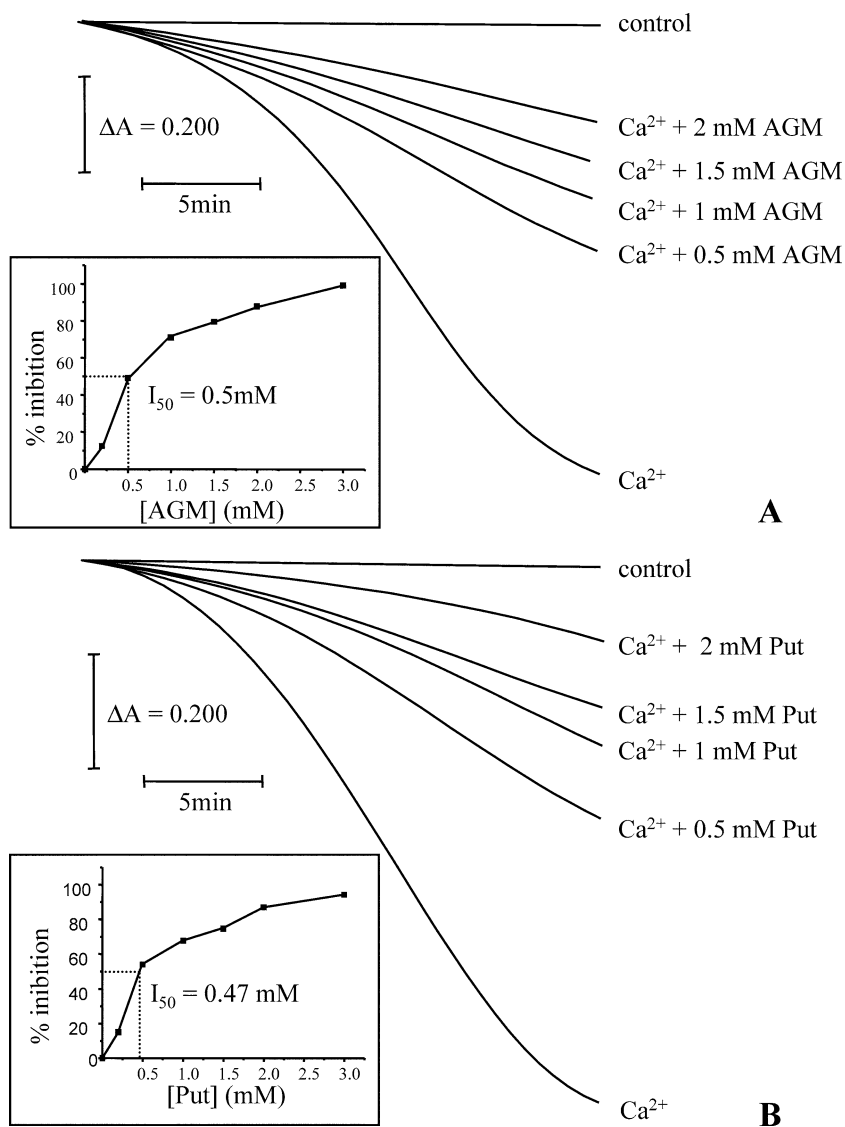
The data represented in Fig. 3 was obtained by five different independent assays. All experimental results are expressed as the mean ± standard deviation (SD).

Results

Biological assays

Agmatine at 15 μmol dm⁻³ concentration was previously reported to induce MPT through a mechanism, which possibly involves generation of H₂O₂ [12]. However, an opposite effect was observed when mitochondria was treated with higher concentrations of agmatine [15]. These observations are corroborated and better explained by the present results. In fact, the biological assays now performed allow to determine that, in the concentration range 0.5–2 mmol dm⁻³, agmatine displays a dose-dependent inhibition on mitochondrial swelling (*I*₅₀ value = 0.5 mmol dm⁻³) (Fig. 2A), almost identical to that detected for the divalent polyamine putrescine (*I*₅₀ = 0.47 mmol dm⁻³) (Fig. 2B). At 1 mmol dm⁻³ concentration, in turn, agmatine was found to prevent the collapse of the membrane potential induced by Ca²⁺ plus phosphate (Fig. 3A), as well as to block the oxidation of sulphhydryl groups (Fig. 3B). Figure 3C reports a Western Blot analysis of mitochondrial cytochrome c in the supernatant, evidencing that concomitantly to the onset of the above mentioned events cytochrome c is also released. The presence of 1 mmol dm⁻³ AGM significantly inhibits this efflux. Furthermore, agmatine showed to be able to inhibit mitochondrial swelling in mitochondria deenergized by carbonyl cyanide p-trifluoromethoxyphenylhydrazone (FCCP), in the presence of ruthenium red (RR), thus suggesting that the amine acts by interacting on the external side of the mitochondrial membrane (Fig. 3D). These observations clearly indicate that agmatine, at high concentrations, inhibits the

Fig. 2 Dose- dependent effect of agmatine (A) and putrescine (B) on mitochondrial swelling induced by Ca^{2+} in the presence of phosphate. RLM were incubated in standard medium supplemented with $30 \mu\text{mol dm}^{-3} \text{Ca}^{2+}$ and 1mmol dm^{-3} phosphate under the conditions described in the Experimental Section. Agmatine (AGM) and putrescine (Put) were present at the indicated concentrations. A downward deflection indicates mitochondrial swelling. The insets show the calculation of the I_{50} values for both agmatine and putrescine. (Four other assays yielded identical results)



triggering of MPT, as opposed to the results previously reported by Gardini and collaborators for low AGM concentrations [12] (for a review on MPT see Ref. [43]).

Previously reported studies demonstrate that the preventive effect of natural and synthetic polyamines on MPT induction is strongly dependent on their electric charge, the concentration of amine needed to inhibit the phenomenon being inversely proportional to its charge [44]. Furthermore, the present results show that agmatine still exhibits its inhibitory effect on MPT under deenergizing conditions (Fig. 3D), evidencing that it can prevent the instauration of MPT by binding to the external side of the membrane, without crossing it. In fact, pore opening under deenergizing conditions has been previously reported elsewhere [45]. In the light of these observations, it is proposed that the species responsible for this protective effect are dicationic AGM structures, the structure of which was obtained by theoretical calculations (see below).

Ab initio MO calculations

A complete geometry optimization by density functional calculations was carried out for agmatine, considering the distinct protonation states of the molecule. The effect of several structural parameters on the overall stability of the polyamine was investigated, namely: (i) conformation of the guanidinium group relative to the carbon chain $(-\text{CH}_2)_4-$ of the molecule—change in the $(\text{C}_4\text{C}_5\text{N}_{16}\text{C}_{18})$ dihedral angle (rotation around the C_5-N_{16} bond) (Fig. 1); (ii) orientation of the guanidinium $(\text{C}_{18}=\text{N})\text{N}-\text{H}$ group relative to the $\text{C}_{18}-\text{N}_{21}$ bond— $(\text{H}_{20}\text{N}_{19}\text{C}_{18}\text{N}_{21})$ dihedral equal to 0 or 180° , defining either a *cis* or a *trans* configuration, respectively.

Both considering the isolated molecule and the aqueous solution, five different conformers were obtained for unprotonated ($n=0$, $q=0$) and monoprotonated ($n=1$, $q=1+$) agmatine, while six were found for the diprotonated ($n=2$, $q=2+$) species (Table 1, Figs. 1 and 4).

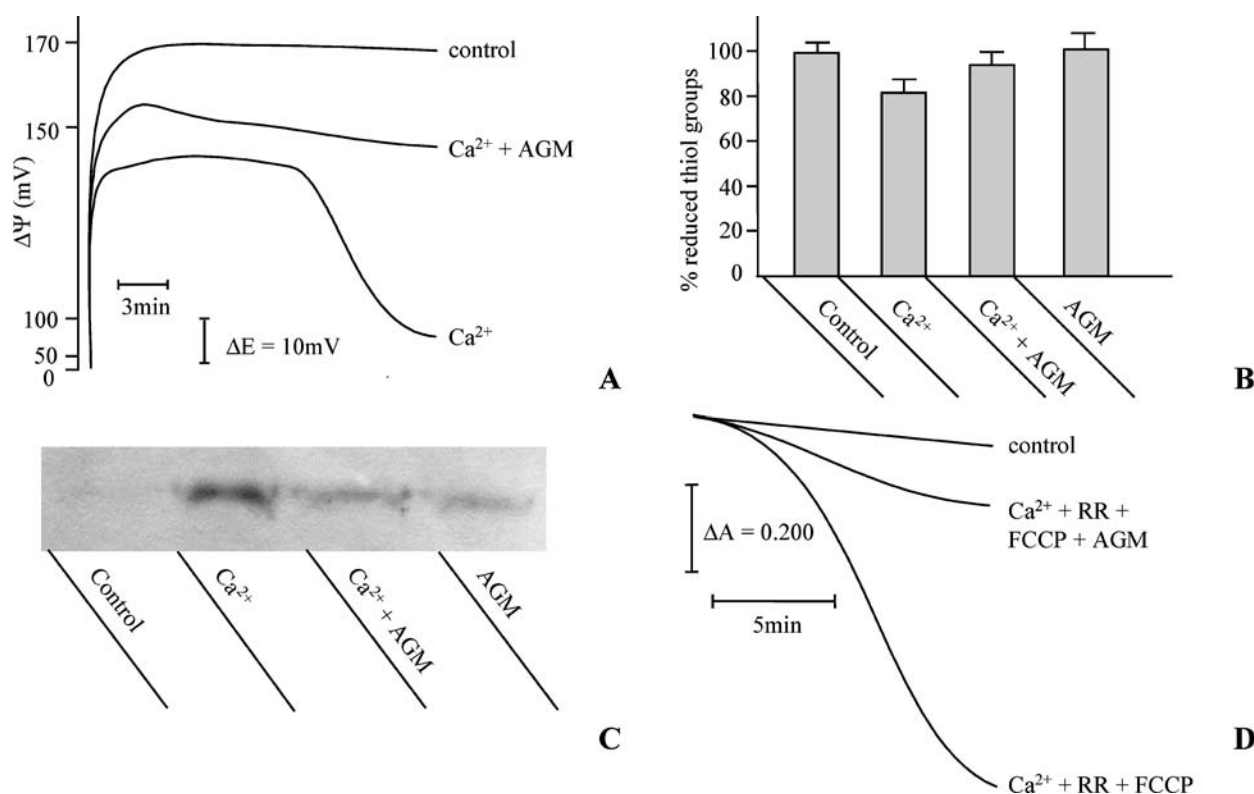


Fig. 3 Protective effect of agmatine on $\Delta\Psi$ collapse (A), thiol oxidation (B), and cytochrome c release (C), induced by Ca^{2+} and phosphate. Protective effect of agmatine on mitochondrial swelling induced by Ca^{2+} plus ruthenium red (RR) and FCCP (D). Panels A–C: RLM was incubated for 20 min (in the same conditions as those described for Fig. 1A). Agmatine was present at 1 mmol dm^{-3} concentration. The ΔE value indicated in panel A refers to the electrode potential. Panel C represents the cytochrome c released from RLM to the supernatant and undergone to SDS-PAGE. The gel was transferred to nitrocellulose

membrane and immunostained with anticytochrome c anti-body. For plots A and C four different assays were performed yielding identical results. The results comprised in panel B are the mean values $\pm 2\text{SD}$ of five different experiments. Panel D: RLM were incubated in standard medium in the presence of $30\text{ }\mu\text{mol dm}^{-3}\text{ Ca}^{2+}$. Where indicated, $0.5\text{ }\mu\text{mol dm}^{-3}$ RR and $0.1\text{ }\mu\text{mol dm}^{-3}$ FCCP (added 2 min after Ca^{2+}) and 1 mmol dm^{-3} agmatine were present. Four other experiments yielded similar results

For the unprotonated species, four conformers were determined to be significantly populated at room temperature (Table 1). The lowest energy geometry (AGM 00) presents a quasi-perpendicular orientation of the guanidinium group ($(\text{C}_4\text{C}_5\text{N}_{16}\text{C}_{18})$ ca. 78.0°) and a *cis* conformation of $(\text{C}_{18}=\text{N})\text{H}$ relative to the $\text{C}_{18}\text{--N}_{21}$ bond (Fig. 4). Conformer AGM 04 was determined to be highly destabilized (mainly for the isolated molecule), most probably due to the orientation of the guanidinium NH_2 relative to the aliphatic amino group (Fig. 4)—AGM 04 vs AGM 03, Table 1.

Three conformations with considerable population at room temperature were obtained for the diprotonated species of agmatine—AGM 22, AGM 23, and AGM 25 (Table 1). The most stable structure in aqueous solution—AGM 22, probably the predominant species at physiological pH—displays a quasi-perpendicular guanidinium group ($(\text{C}_4\text{C}_5\text{N}_{16}\text{C}_{18}) = -89.0^\circ$, Table 2) relative to the carbon chain, as opposed to the lowest energy conformer for the isolated molecule, AGM 23, which has a $(\text{C}_4\text{C}_5\text{N}_{16}\text{C}_{18})$ dihedral of 165.6° . In both cases, the $(\text{C}_{18}=\text{N})\text{H}$ group

adopts a *trans* orientation relative to the $\text{C}_{18}\text{--N}_{21}$ bond. The two species present in aqueous solution with almost identical populations, AGM 22 (37.2%) and AGM 25 (36.0%), are enantiomeric conformations, varying solely in the relative orientation of the guanidinium group and the aliphatic chain— $(\text{C}_4\text{C}_5\text{N}_{16}\text{C}_{18})$ equal to $\pm 89.0^\circ$ (Tables 1 and 2, Fig. 5).

Regarding the monoprotonated molecule (protonated only in the guanidinium amino group, displaying the highest polarity), two mainly populated geometries (at room temperature) were obtained—AGM 10 and AGM 11 (Table 1, Fig. 5). Similarly to what has been verified for diprotonated agmatine, while the minimum energy conformer for the isolated molecule (AGM 11, Fig. 4) displays a coplanar structure, a tilted conformation (AGM 10, Fig. 5) was found to be the most favoured one in solution. A *trans* guanidinium $(\text{C}_{18}=\text{N})\text{H}$ group relative to $\text{C}_{18}\text{--N}_{21}$ was also determined to lead to a higher stabilization. The highest energy conformer (AGM 14), in turn, presents two conformational characteristics which were found to be energetically unfavoured: a *cis*

Table 1 Calculated relative energies, populations, and dipole moments (μ) for the distinct conformers of agmatine, in its distinct protonation states, both as an isolated molecule and in aqueous solution

Conformer	ΔE , kJ mol ⁻¹ (population ^a , %)		IEFPCM	
	B3LYP/6-31G** ^b	μ/D^c	B3LYP/6-31G** ^d	μ/D
<i>n</i> = 0 (<i>q</i> = 0) ^e				
AGM 00	0 (38.6)	3.5	0 (35.7)	4.9
AGM 01	2.1 (16.4)	2.4	0.3 (31.7)	3.6
AGM 02	1.7 (19.6)	3.5	1.9 (16.5)	5.1
AGM 03	1.1 (24.9)	1.7	2.3 (13.9)	2.8
AGM 04	10.6 (0.5)	3.3	6.9 (2.2)	4.4
<i>n</i> = 1 (<i>q</i> = 1 +)				
AGM 10	1.7 (33.7)	13.4	0 (54.7)	15.8
AGM 11	0 (66.3)	13.0	0.9 (38.5)	15.2
AGM 12	27.2 (0)	16.0	6.5 (3.9)	19.3
AGM 13	26.7 (0)	15.9	7.3 (2.9)	19.1
AGM 14	32.5 (0)	12.9	21.7 (0)	15.2
<i>n</i> = 2 (<i>q</i> = 2 +)				
AGM 20	9.2 (1.1)	2.7	5.1 (4.7)	5.1
AGM 21	12.5 (0.3)	4.5	7.1 (2.1)	6.6
AGM 22	1.4 (26.4)	5.9	0 (37.2)	7.2
AGM 23	0 (46.4)	7.1	1.6 (19.5)	8.9
AGM 24	18.3 (0)	10.0	10.7 (0.5)	12.5
AGM 25	1.5 (25.8)	5.9	0.1 (36.0)	7.3

^aCalculated at 25°C.

^bIsolated molecule.

^c1D = 1/3 × 10⁻² cm.

^dIn water, $\epsilon^{25^\circ\text{C}} = 78.39$.

^e*n* represents the protonation state of the molecule, while *q* refers to its charge.

orientation of the guanidinium (C₁₈=)N–H relative to the C₁₈–N₂₁ bond, coupled to a *trans* (C₁₈=)NH relative to the aliphatic NH₃⁺. Thus, despite its high dipole moment ($\mu = 15.2$ D), this geometry is not populated in aqueous solution at room temperature, as opposed to AGM 11, which has an identical polarity ($\mu = 15.2$ D) but a population of 38.5% (Table 1).

Similarly to what has been reported for putrescine [46, 47], the carbon chain of the agmatine molecule was found to adopt a preferential linear *all-trans* configuration, for all protonation states of the molecule. A *trans* orientation of the guanidinium (C₁₈=)N–H relative to the C₁₈–N₂₁ bond was found to be energetically favored whenever the neighbouring amino moiety is protonated, which is easily understandable in the light of minimisation of the H₂₀···H₂₃ steric repulsions: conformers AGM 10 *vs.* AGM 12, AGM 11 *vs.* AGM 13, AGM 22 and AGM 25 *vs.* AGM 20, and AGM 23 *vs.* AGM 21 (Fig. 4). Moreover, a *trans* conformation of the (C₁₈=)NH moiety relative to the aliphatic NH₂ ((C₅N₁₆C₁₈N₁₉) *ca.* 180.0°) is clearly unfavored: conformers AGM 04 *vs.* AGM 03, AGM 14 *vs.* AGM 13, AGM 24 *vs.* AGM 23 (Fig. 4). In aqueous solution, those geometries displaying a nonplanar conformation of the guanidinium group relative to the carbon chain showed to be stabilized relative to the coplanar ones (which are favored for the isolated molecule).

Apart from the relative orientation of the N₁₉–H₂₀ and C₁₈–N₂₁ bonds (Fig. 1), the configuration of the whole guanidinium (C₁₈=)NH moiety relative to the aliphatic amine chain thus proved to be a quite important parameter for the stabilization of the agmatine molecule, most probably due

to electronic delocalization factors. In fact, by comparing the results obtained for the isolated agmatine (gas phase) and considering the presence of water, it may be concluded that the nonplanar geometries are clearly favored in solution (AGM 00 *vs.* AGM 01 and AGM 10 *vs.* AGM 11 Fig. 5, Table 1).

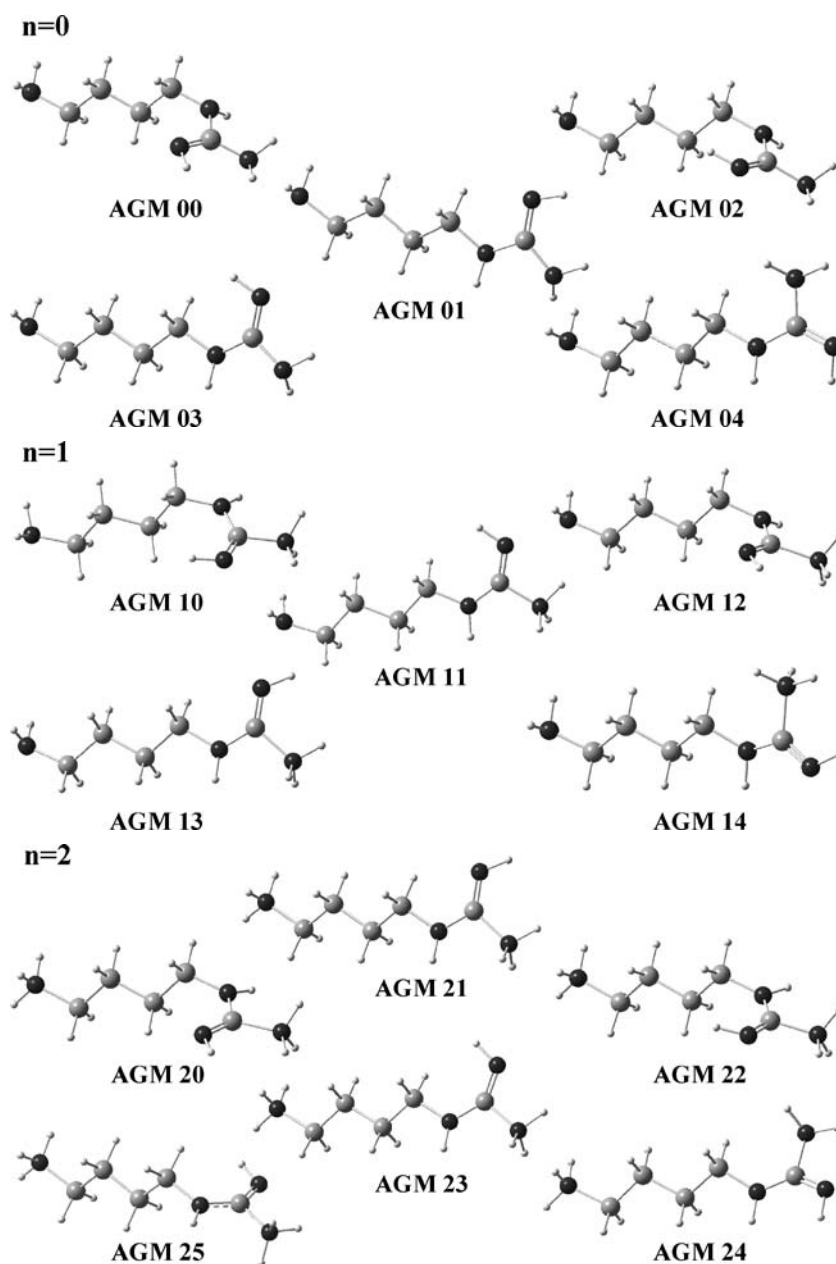
N-Protonation of agmatine, in turn, was found to lead to an expected decrease of the negative charge of the nitrogen atoms, both for the guanidinium moiety of the molecule and for the terminal amino group: uncharged conformers *vs.* mono- and dipositive species, and monoprotinated *vs.* diprotinated forms (Fig. 5). As to the carbon atoms adjacent to the ionizable site, while the guanidinium C₁₈ is unaffected by protonation, the charge in C₂ is approximately doubled (–0.06 to –0.12) upon N₁-protonation (Fig. 5).

Raman spectroscopy

The Raman spectra (100–1750 cm⁻¹) of diprotinated agmatine, both in the solid state and in aqueous solution (at pH 7.3), are represented in Fig. 6. Figure 7 comprises the Raman pattern of agmatine aqueous solutions (*ca.* 0.5 mol dm⁻³), at distinct pH values. The corresponding experimental wavenumbers are listed in Table 3, along with the calculated frequencies for the most stable conformers of the diprotinated molecule—AGM 23 (isolated amine) and AGM 22 (aqueous solution).

A complete assignment of the experimental vibrational features was carried out (Table 3), in the light of both the theoretical results and the spectra of the similar polyamines dien (H₂N(CH₂)₂NH(CH₂)₂NH₂) and propen

Fig. 4 Schematic representation of the calculated (B3LYP/6-31G**) lowest energy conformers for isolated agmatine, in its distinct protonation states



($\text{H}_2\text{N}(\text{CH}_2)_3\text{NH}(\text{CH}_2)_3\text{NH}_2$) presently obtained (Fig. 8), as well as based on the data previously gathered for the analogous biogenic amines putrescine ($\text{H}_2\text{N}(\text{CH}_2)_4\text{NH}_2$), spermidine ($\text{H}_2\text{N}(\text{CH}_2)_3\text{NH}(\text{CH}_2)_4\text{NH}_2$), and spermine ($\text{H}_2\text{N}(\text{CH}_2)_3\text{NH}(\text{CH}_2)_4\text{NH}(\text{CH}_2)_3\text{NH}_2$) [46–49].

The vibrational results now reported for agmatine are in total agreement with its theoretically determined conformational behavior, previously described. In fact, the expected structural changes due to *N*-protonation are clearly detected in its Raman spectra: as pH is increased (and the amount of protonated species gets lower and lower) a strong decrease in intensity is observed for the very intense band at 983 cm^{-1}

(Fig. 7), ascribed to a deformation (rocking) mode of the NH_3^+ guanidinium group, ρ_{NH_3} (Table 3). Moreover, as the percentage of the unprotonated form raises the broad feature at *ca.* 1650 cm^{-1} , assigned to the NH_2 scissoring mode, increases in intensity. It should be noted that at pH 11.8 there is still a nonnegligible percentage of monoprotated agmatine in solution, which accounts for the presence of the band at 983 cm^{-1} , although much weaker than for lower pH values, when the dipositive species is predominant in solution (Fig. 7). The occurrence of the Raman strong feature due to the ρ_{NH_3} mode is predicted by the calculations, for the mono- and dipositive forms of agmatine (displaying a protonated

Table 2 Optimized geometries for the most stable conformers of agmatine at physiological conditions (B3LYP//6-31G** level of calculation)

	AGM 22	AGM 25
Bond lengths (pm)		
N ₁ –C ₂ ^a	150.8	150.7
N ₁₆ –C ₁₈	135.0	135.0
C ₁₈ –N ₁₉	126.9	127.0
C ₁₈ –N ₂₁	149.8	149.8
C ₂ –C ₃	152.4	152.4
C ₃ –C ₄	153.5	153.5
C ₄ –C ₅	153.5	153.5
N ₁ –H ₆	103.4	103.4
N ₁ –H ₇	103.4	103.4
N ₁ –H ₂₅	103.4	103.4
N ₁₆ –H ₁₇	102.6	102.6
N ₁₉ –H ₂₀	102.3	102.3
N ₂₁ –H ₂₂	103.7	103.7
N ₂₁ –H ₂₃	103.7	103.7
N ₂₁ –H ₂₄	103.4	103.4
C ₂ –H ₈	109.3	109.3
C ₂ –H ₉	109.3	109.3
C ₃ –H ₁₀	109.8	109.9
C ₃ –H ₁₁	109.8	109.8
C ₄ –H ₁₂	109.7	109.7
C ₄ –H ₁₃	109.7	109.7
C ₅ –H ₁₄	109.6	109.5
C ₅ –H ₁₅	109.5	109.6
Bond angles (°)		
N ₁₆ –C ₁₈ –N ₁₉	135.1	135.1
N ₁₉ –C ₁₈ –N ₂₁	113.6	113.6
N ₁ –C ₂ –C ₃	111.0	111.1
C ₄ –C ₅ –N ₁₆	113.1	113.1
C ₂ –C ₃ –C ₄	111.1	111.0
C ₃ –C ₄ –C ₅	111.5	111.5
N ₁ –C ₂ –H ₈	106.3	106.3
C ₂ –N ₁ –H ₆	111.7	111.7
C ₂ –N ₁ –H ₇	111.7	111.7
C ₅ –N ₁₆ –H ₁₇	116.8	111.9
C ₁₈ –N ₁₉ –H ₂₀	113.6	113.6
C ₁₈ –N ₂₁ –H ₂₂	112.0	112.1
C ₁₈ –N ₂₁ –H ₂₃	107.9	108.0
C ₂ –C ₃ –H ₁₀	109.4	109.4
C ₃ –C ₄ –H ₁₂	109.9	109.9
C ₄ –C ₅ –H ₁₄	110.6	110.9
Dihedral angles (°)		
C ₅ –N ₁₆ –C ₁₈ –N ₁₉	–5.3	5.2
C ₅ –N ₁₆ –C ₁₈ –N ₂₁	176.6	176.7
N ₁ –C ₂ –C ₃ –C ₄	179.6	179.8
C ₂ –C ₃ –C ₄ –C ₅	179.6	–179.6
C ₃ –C ₄ –C ₅ –N ₁₆	–179.8	178.7
C ₄ –C ₅ –N ₁₆ –C ₁₈	–89.0	–88.6
N ₁₆ –C ₁₈ –N ₁₉ –H ₂₀	1.9	–1.6
N ₁₆ –C ₁₈ –N ₂₁ –H ₂₂	58.5	–178.4
N ₁₆ –C ₁₈ –N ₂₁ –H ₂₃	178.0	62.2
C ₃ –C ₂ –N ₁ –H ₆	–59.9	–60.3
C ₃ –C ₂ –N ₁ –H ₇	60.3	59.9
N ₁ –C ₂ –C ₃ –H ₁₀	52.2	58.5

Table 2 Continued

	AGM 22	AGM 25
C ₄ –C ₃ –C ₂ –H ₈	60.9	61.1
C ₂ –C ₃ –C ₄ –H ₁₂	–59.0	–58.6
C ₃ –C ₄ –C ₅ –H ₁₄	58.3	58.8

^aAtoms are numbered according to Fig. 1.

guanidinium group, Fig. 5), both for the isolated molecule and for the aqueous solution, at 994 and 981 cm⁻¹, respectively (Table 3). The protonation state of agmatine can thus be easily and unequivocally determined through its Raman pattern, in aqueous solution.

Discussion

The results gathered along the present study lead to the understanding of the conformational preferences of agmatine, namely to the determination of the most stable physiological agmatine structures, i.e., the predominant species present in aqueous solution at pH 7.3. These were found to be the dicationic forms AGM 22 and AGM 25, displaying a lower negative charge in the protonated aliphatic amino terminal relative to the monoprotonated or neutral forms of the molecule (Fig. 5). Most probably, these are also the conformations to be found in the biological fluids during agmatine absorption from the diet, as well as in the cytosol, in mammalian cells, after agmatine is transported across the plasma membrane. Consequently, these are prone to be the species that interact with the mitochondrial membrane and have a marked effect on MPT, a phenomenon known to be associated with apoptosis (for a review see Ref. [16]).

The concentration-dependent effect of agmatine on MPT induction verified along this work may be explained by considering that it is due to the oxidation products of agmatine (H₂O and aldehyde) in the presence of Ca²⁺. Thus, while for low AGM concentrations all the amine is in the oxidized form, at high concentrations the tendency toward pore opening triggered by the oxidation of agmatine is counteracted, or even abolished, by the intact amine molecules, not yet oxidized. These results are in accordance with those found in the literature for the monoamine tyramine [50].

Although no specific agmatine transport mechanism has, to this date, been characterized at a molecular level, there are several proposed models reported in the literature. One of these suggests that agmatine may (e.g., in human cell lines derived from embryonic kidney) be transported through the nonneuronal monoamine transporters EMT and OCT2 [14]. In this particular case, it was verified that the transport velocity is directly proportional to the concentration of

Fig. 5 Schematic representation of the calculated (IEFPCM/B3LYP/6-31G**) lowest energy conformers for agmatine in aqueous solution, in its distinct protonation states. (Mulliken atomic charges are included. The most abundant physiological forms of agmatine are AGM 22 and AGM 25)

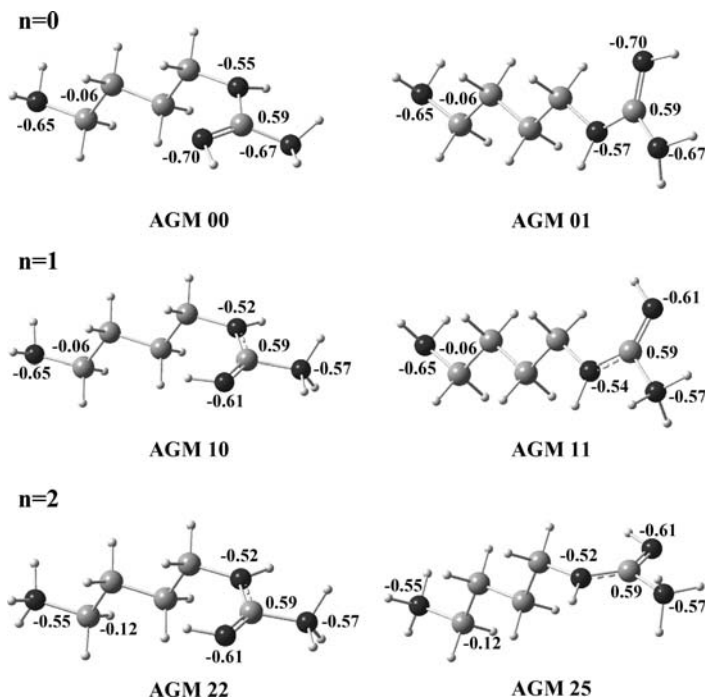


Fig. 6 Experimental Raman spectra ($100\text{--}1750\text{ cm}^{-1}$) of diprotonated agmatine (at 25°C): (A) solid state; (B) aqueous solution (0.5 mol dm^{-3} , pH 7.3). (δ and ρ represent deformation and rocking vibrational modes, respectively; atoms are numbered according to Fig. 1)

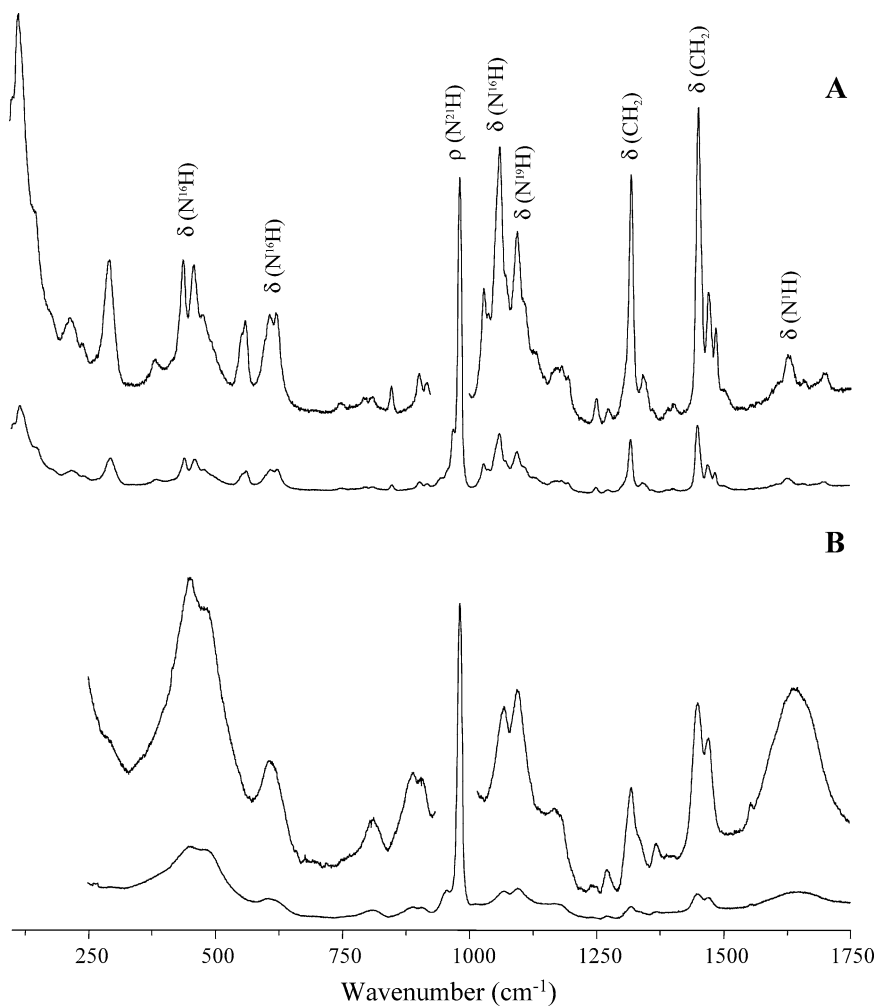


Table 3 Raman experimental and calculated wavenumbers (cm^{-1}) for diprotonated agmatine (Physiological species), both in the solid state and in aqueous solution

	Experimental		Calculated ^a		Approximate description ^b
	Solid state	Aqueous solution ^c	Isolated molecule ^d	Aqueous solution ^e	
	3389		3444	3327	ν (N^{19}H)
	3332		3438	3305	ν (N^{16}H)
	3273		3343	3271	ν_{as} (N^{21}H_3)
	3183		3339	3270	ν_{as} (N^1H_3) + ν_{as} (N^{21}H_3)
	2996		2989	2997	ν_{as} (CH_2)
	2973	2977	2982	2972	ν_{s} (CH_2)
	2947	2934	2959	2949	ν_{as} (CH_2)
	2925	2905	2928	2946	ν_{s} (CH_2)
	2876	2884	2918	2924	ν_{s} (CH_2)
	2795	2792	2917	2910	ν_{s} (CH_2)
	1698		1756	1722	ν ($\text{C}^{18}=\text{N}^{19}$)
	1627	1647	1607	1613	δ_{as} (N^1H_3)
	1473	1472	1471	1468	δ (CH_2)
	1451	1448	1449	1448	δ (CH_2)
	1341		1334	1342	δ (CH_2)
	1319	1318	1313	1323	δ (CH_2)
	1195		1219	1229	δ (CH_2) + δ (N^{16}H) ^{ip} + δ (N^{19}H) ^{ip}
	1182	1173	1206		δ (CH_2) + δ (N^{16}H) ^{ip} + δ (N^{19}H) ^{ip}
	1095	1095	1111	1123	ν ($\text{C}-\text{C}$)
	1063	1068	1047	1071	ρ (N^{21}H_3) + δ (N^{19}H) ^{op}
	1027		1033	1058	ρ (N^{21}H_3) + ρ (N^1H_3) + δ (CH_2)
	983	983	994	981	ρ (N^{21}H_3)
	969	952	964	958	ν ($\text{C}-\text{C}$) + ν ($\text{C}-\text{N}$)
		912	940	934	ν ($\text{C}-\text{C}$) + ν ($\text{C}-\text{N}$) + ρ (N^{21}H_3) + δ (N^{19}H_3) ^{ip}
		891	909	883	ν ($\text{C}-\text{C}$) + ν ($\text{C}-\text{N}$) + δ (CH_2)
		810	795	811	δ (CH_2) + δ (N^{19}H_3) ^{op}
	608	606		601	δ (N^{16}H) ^{op}
	560		565	579	δ (N^{16}H) ^{op} + ν ($\text{N}-\text{C}-\text{N}$)
	461	487	485	464	δ (N^{16}H) ^{op}
	442	449	429	425	ν ($\text{C}-\text{C}$) + ν ($\text{C}-\text{N}$)
	385		402	344	τ (N^1H_3)
	294	296	347	322	τ (N^{21}H_3)
	219		234	286	Skeletal mode
	150		164	150	Skeletal mode
	116		123	144	Skeletal mode

^aB3LYP/6-31G** level, for the isolated molecule; IEFPCM/B3LYP/6-31G** level, for the aqueous solution; wavenumbers above 400 cm^{-1} are scaled by 0.9614 [36].

^bAtoms are numbered according to Fig. 1; the vibrational modes are represented by: ν , stretching; δ , deformation; ρ , rocking and τ , torsion; ip and op stand for in-plane and out-of-plane modes.

^cpH is 7.3.

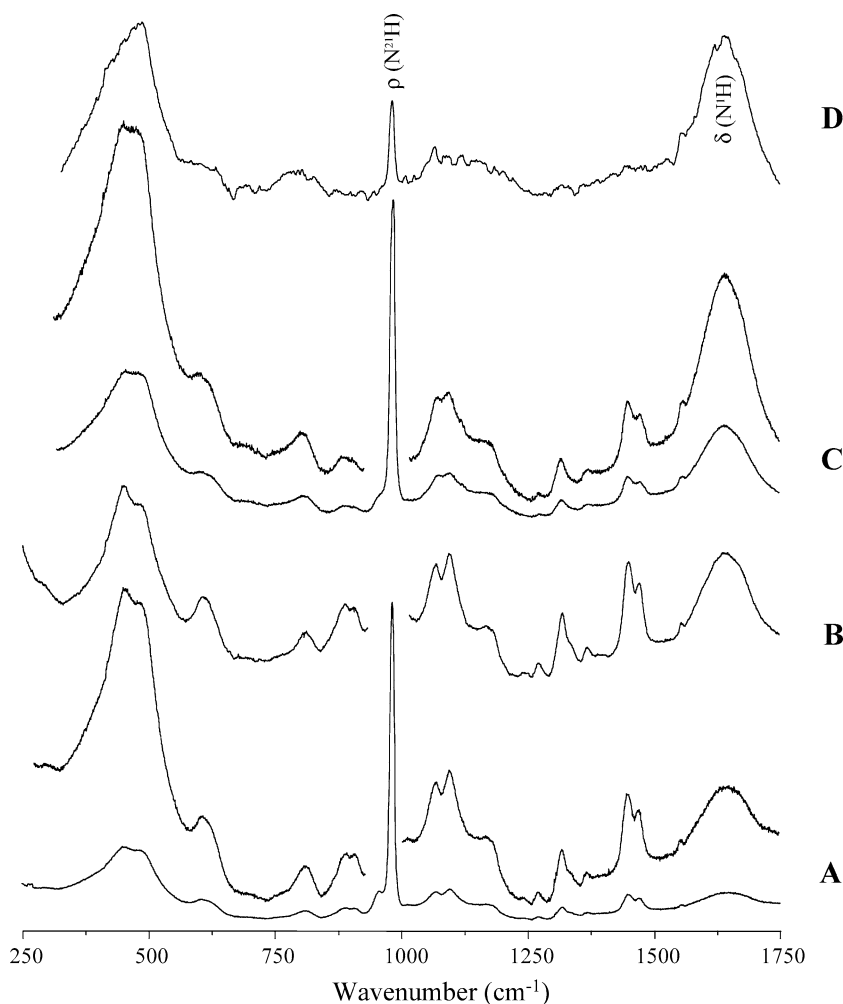
^dAGM 23 conformer.

^eAGM 22 conformer.

the monoprotonated form of the molecule, the uptake increasing drastically with increasing pH (in the range 6.5–9.0). Thus, the monoprotonated species AGM 10 and AGM 11 (Fig. 5) would be the sole substrates for either EMT or OCT2. However, this behavior seems to indicate that this transport mechanism is most likely an electroneutral one, and consequently the amine should not be transported in the monoprotonated form (which has a quite high dipole moment), as proposed by Grundemann and collaborators [14], but instead in the totally unprotonated, uncharged form—AGM 00 and AGM 01 (Fig. 5). In turn, if a hydrophilic channel is considered as the specific transport system, agmatine

should be in the diprotonated state—AGM 22 and AGM 25 (Fig. 5)—which has a dipole moment of about one-half that of the monoprotonated species (Table 1). A specific transport system for agmatine in mitochondria has recently been identified [15] as being a strictly electrophoretic mechanism, exhibiting a V_{max} value ($6.5 \text{ nmol min}^{-1} \text{ mg}^{-1} \text{ prot}$) about 5-fold higher than the corresponding one for the analogous divalent biogenic amine putrescine ($[\text{H}_3\text{N}(\text{CH}_2)_4\text{NH}_3]^{2+}$, $V_{\text{max}} = 1.14 \text{ nmol min}^{-1} \text{ mg}^{-1} \text{ prot}$) [51]. Since this transporter resembles that of putrescine, a hydrophilic channel is known to be involved and the agmatine conformers capable of crossing the mitochondrial membrane should then be the

Fig. 7 Experimental Raman spectra ($100\text{--}1750\text{ cm}^{-1}$) of agmatine in aqueous solution, as a function of pH (0.5 mol dm^{-3} , 25°C): (A) pH 4.5; (B) pH 7.3; (C) pH 10.1; (D) pH 11.8. (δ and ρ represent deformation and rocking vibrational modes, respectively; atoms are numbered according to Fig. 1)



diprotonated ones AGM 22 and AGM 25 (Fig. 5). Nevertheless, the large difference between the measured transport rates for agmatine and putrescine are suggested to be indicative of an alkaline microenvironment of the agmatine transporter ($\text{pH} > 7.3$), which will imply that this amine is not carried as a dipositive species, but as a monovalent, high dipole moment, cation instead (AGM 10 and AGM 11).

Considering the occurrence of electrostatic interactions between agmatine and the fixed anionic charges of neighboring biological structures (e.g., aspartic and/or glutamic acid residues from transporter proteins, Fig. 9), the most probable conformations for this polyamine under physiological conditions are the dipositive ones AGM 22 and AGM 25 (as also suggested by the results on MPT triggering), although the monocationic species AGM 10 and AGM 11 may also exist in particular microenvironments. However, agmatine is also known to interact with hydrophobic sites *in vivo*, in which case the structures involved would be AGM 00 and AGM 01, which are the most abundant uncharged forms in solution.

Conclusions

The results obtained along the present study allowed to thoroughly characterize the structure of the most stable geometries of agmatine in aqueous solution, under different pH conditions (Fig. 5): at physiological pH, the diprotonated (dipositive) forms—AGM 22 and AGM 25; at alkaline pH (*ca.* 7.3–9.0), the monoprotated (monopositive) species—AGM 10 and AGM 11; and in strong alkaline medium, the totally unprotonated (neutral) molecule—AGM 00 and AGM 01.

Since the activity of biogenic polyamines is recognized to be strongly affected by their structural preferences, the determination of the conformational behavior of agmatine is of the utmost importance for the understanding of its diverse biological roles, namely its effect on the mitochondrial permeability transition and its specific transport mechanism. These SAR's studies are essential for the development of new agmatine-based therapeutic strategies (e.g., against drug addiction, pain-killing, or tumor suppressing).

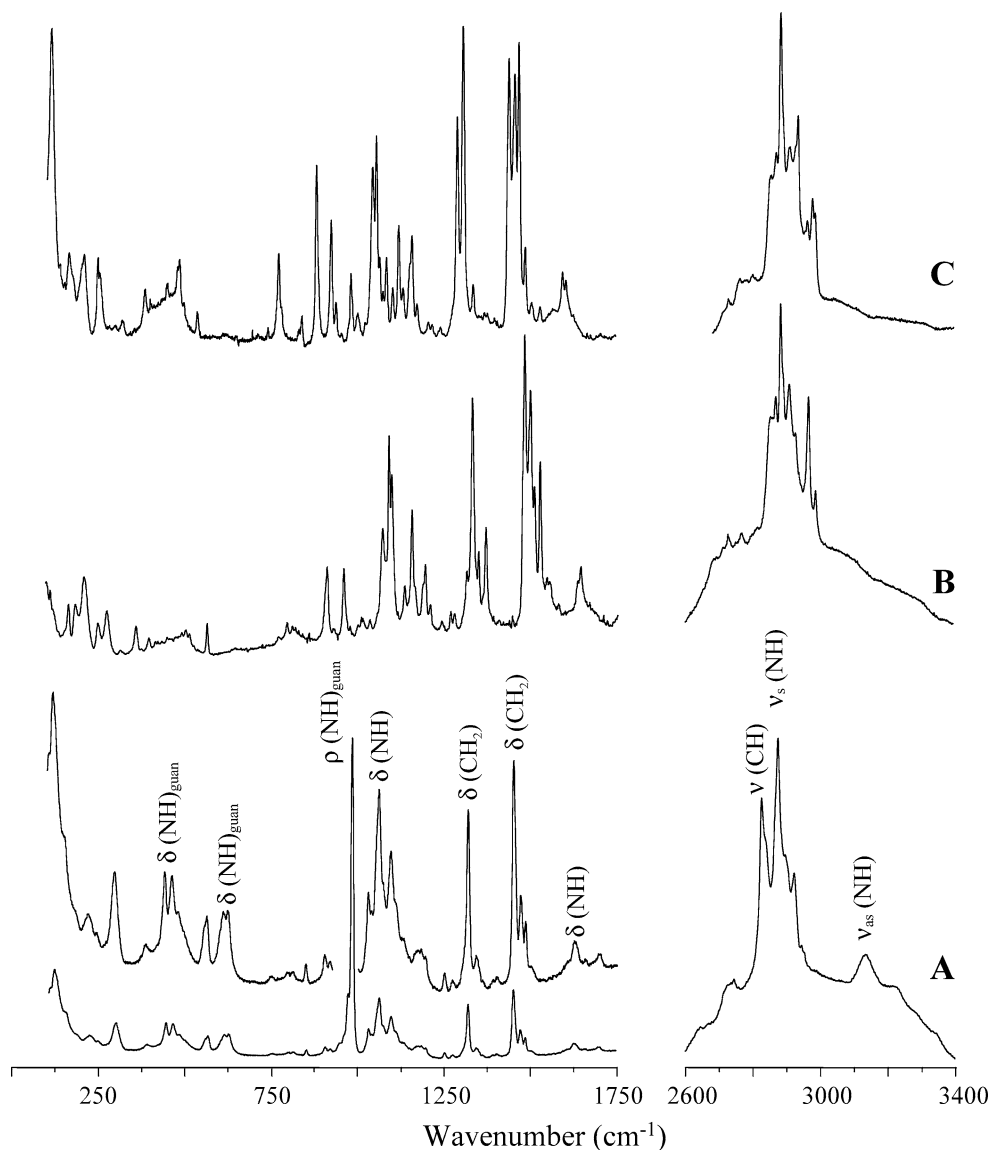


Fig. 8 Experimental Raman spectra (100–1750, 2600–3400 cm^{-1}) of agmatine (A), dien (B), and propen (C), in their totally protonated forms (solid state, at 25°C). (The vibrational modes are represented by:

ν , stretching; δ , deformation; and ρ , rocking; s and as stand for symmetric and antisymmetric vibrations; *guan* refers to the guanidinium moiety of the molecule; atoms are numbered according to Fig. 1)

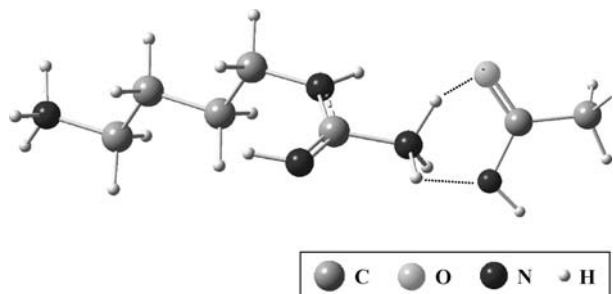


Fig. 9 Schematic representation of the possible interaction between acidic amino acid terminals (e.g., from a transport protein) and the most stable structure of agmatine at physiological conditions (dicationic species AGM 22)

Acknowledgements Work performed within the COST Action 922 from the European Science Foundation. RC and VB acknowledge financial support, respectively, from the Portuguese Foundation for Science and Technology—PhD fellowship SFRH//BD/16520/2004—and from the European Science Foundation—COST-STSM-922-00620 (study mainly developed in the Research Unit “Molecular Physical-Chemistry,” Portugal).

References

1. Raasch W, Regunathan S, Li G, Reis D (1995) *J Life Sci* 56:2319
2. Grillo MA, Colombatto S (2004) *Amino Acids* 26:3
3. Li G, Regunathan S, Barrow CJ, Eshraghi J, Cooper R, Reis D (1994) *J Sci* 263:966
4. Piletz JE, Chikkala DN, Emsberger P (1995) *J Pharmacol Exp Ther* 272:581

5. Raasch W, Schafer U, Chun J, Dominiak P (2001) *Br J Pharm* 133:755
6. Sener A, Lebrun F, Blaicher F, Malaisse W (1989) *J Biochem Pharmacol* 38:327
7. Satriano J, Matsufuji S, Murakami Y, Lortie MJ, Schwartz D, Kelly CJ, Hayashi SI, Blantz RC (1998) *J Biol Chem* 273:15313
8. Satriano J, Kelly CJ, Blantz RC (1999) *Kidney Int* 56:1252
9. Dudkowska M, Lai J, Gardini G, Stachurska A, Grzelakowska-Sztabert B, Colombatto S, Manteuffel-Cymborowska M (2003) *Biophys Biochim Acta* 1619:159
10. Higashi K, Yoshida K, Nishimura K, Momiyama E, Kashiwagi K, Matsufuji S, Shirahata A, Igarashi K (2004) *J Biochem* 136:533
11. Gardini G, Cravanzola C, Autelli R, Testore G, Cesa R, Morando L, Solinas SP, Muzio G, Grillo MA, Colombatto S (2003) *J Hepatol* 39:793
12. Gardini G, Cabella C, Cravanzola C, Vargiu C, Belliardo S, Testore G, Solinas SP, Toninello A, Grillo MA, Colombatto S (2001) *J Hepatol* 35:482
13. Satriano J, Isome M, Casero RA Jr, Thomson SC, Blantz RC (2001) *Am J Physiol Cell Physiol* 281:C329
14. Grundemann D, Hahne C, Berkels R, Schomig E (2003) *J Pharmacol Exp Ther* 304:810
15. Salvi M, Bedino S, Mancon M, Colombatto S, Grillo MA, Toninello A (2004) Agmatine transport in liver mitochondria, in COST 922: health implications of dietary amines. Alberé di Tenna, Italy, p 8
16. Zoratti M, Szabó I (1995) *BBA* 1241:139
17. Green DR, Kroemer G (2004) *Science* 305:626
18. Schneider WC, Hogeboom GH (1950) *J Biol Chem* 183:123
19. Gornall AG, Bardawill CJ, David MM (1949) *J Biol Chem* 177:751
20. Toninello A, Salvi M, Colombo L (2000) *J Exp Biol* 203:3425
21. Santos AC, Uyemura SA, Lopes JL, Bazon JN, Mingatto FE, Curti C (1998) *Free Radic Biol Med* 24:1455
22. Frisch MJ, Trucks GW, Schlegel HB, Scuseria GE, Robb MA, Cheeseman JR, Zakrzewski VG, Montgomery JA Jr, Stratmann RE, Burant JC, Dapprich S, Millam JM, Daniels AD, Kudin KN, Strain MC, Farkas O, Tomasi J, Barone V, Cossi M, Cammi R, Mennucci B, Pomelli C, Adamo C, Clifford S, Ochterski J, Petersson GA, Ayala PY, Cui Q, Morokuma K, Malick DK, Rabuck AD, Raghavachari K, Foresman JB, Cioslowski J, Ortiz JV, Baboul AG, Stefanov BB, Liu G, Liashenko A, Piskorz P, Komaromi I, Gomperts R, Martin RL, Fox DJ, Keith T, Al-Laham MA, Peng CY, Nanayakkara A, Challacombe M, Gill PMW, Johnson B, Chen W, Wong MW, Andres JL, Gonzalez C, Head-Gordon M, Replogle ES, Pople JA (1998) *Gaussian 98, Revision A.9*. Gaussian Inc., Pittsburgh, PA, USA
23. Russo TV, Martin RL, Hay PJ (1995) *J Phys Chem* 99:17085
24. Ignaczak A, Gomes JANF (1996) *Chem Phys Lett* 257:609
25. Cotton FA, Feng X (1997) *J Am Chem Soc* 119:7514
26. Ignaczak A, Gomes JANF (1997) *J Electroanal Chem* 420:209
27. Wagener T, Frenking G (1998) *Inorg Chem* 37:1805
28. Cotton FA, Feng X (1998) *J Am Chem Soc* 120:3387
29. Lee C, Yang W, Parr RG (1988) *Phys Rev B* 37:785
30. Miehllich B, Savin A, Stoll H, Preuss H (1989) *Chem Phys Lett* 157:200
31. Becke AD (1988) *Phys Rev A* 38:3098
32. Becke AD (1993) *J Chem Phys* 98:5648
33. Hariharan PC, Pople JA (1973) *Theor Chim Acta* 28:213
34. Franci MM, Pietro WJ, Hehre WJ, Binkley JS, Gordon MS, DeFrees DJ, Pople JA (1982) *J Chem Phys* 77:3654
35. Peng C, Ayala PY, Schlegel HB, Frisch MJ (1996) *J Comp Chem* 17:49
36. Scott AP, Radom L (1996) *J Phys Chem* 100:16502
37. Cancès E, Mennucci B, Tomasi J (1997) *J Chem Phys* 107:3032
38. Mennucci B, Cancès E, Tomasi J (1997) *J Phys Chem B* 101:10506
39. Cancès E, Mennucci B (1998) *J Math Chem* 23:309
40. Barone V, Cossi M, Tomasi J (1998) *J Comp Chem* 19:404
41. Cammi R, Tomasi J (1995) *J Comp Chem* 16:1449
42. Mierts S, Scrocco E, Tomasi J (1981) *J Chem Phys* 55:117
43. Kim JS, He L, Qian T, Lemasters J (2003) *J Curr Mol Med* 3:527–535
44. Tassani V, Biban C, Toninello A, Siliprandi D (1995) *Biochem Biophys Res Commun* 207:661
45. Petronilli V, Cola C, Bernardi P (1993) *J Biol Chem* 268:1011–1016
46. Marques MPM, Batista de Carvalho LAE (2000) In: Morgan DML, White A, Sánchez-Jiménez F, Bardocz S (eds) *Theoretical approach to the conformational preferences of putrescine in COST 917: biogenically active amines in food*, European Commission, vol. IV. Luxembourg, pp 122–129
47. Amorim da Costa AM, Marques MPM, Batista de Carvalho LAE (2003) *J Raman Spectrosc* 34:357
48. Marques MPM, Batista de Carvalho LAE, Tomkinson J (2002) *J Phys Chem A* 106:2473
49. Amorim da Costa AM, Batista de Carvalho LAE, Marques MPM (2004) *Vib Spectrosc* 35:165
50. Marcocci L, Marchi U, Salvi M, Micella ZG, Nocera S, Agostinelli E, Mondovi B, Toninello A (2002) *J Membr Biol* 188:23
51. Toninello A, Dalla Via L, Siliprandi D, Garlid KD (1992) *J Biol Chem* 267:18393